Supplementary Information

Ryota Ohara, Toshiki Iwasaki, and Takeshi Yamazaki

1. Description of Fig. S1

To confirm which of the two terms on the right-hand side in Eq. (6) mainly contributed to the decrease in the cold airmass amounts, the contribution of these two terms was calculated. Figure S1 illustrates daily averages of contributions to the temporal change in cold airmass amounts below the 299 K surface due to the (a), (b) first and (c), (d) second terms in Eq. (6) on 5 and 6 July 2018, respectively. Focusing on the area near the tip of the 299 K surface (near the southern coast of western Japan), the contribution of the first term was almost zero or slightly negative. On the other hand, that of the second term was clearly negative. This means that the northward advection by southerly wind mainly contributed to the decrease in the cold airmass amounts.

2. Description of Fig. S2

Based on the same definition as that in section 3.2, we identified a frontal surface in CNTL to apply the same cold airmass analysis as the analysis using JRA-55. Figure S2 shows the meridional vertical cross-sections of potential temperature averaged from 132°E to 135°E every 12 h from 00UTC on 4 to 12UTC on 5 July 2018 in CNTL. The 300 K isentropic surface was identified as the frontal surface. At 00UTC on 4 July, as shown in Fig. 2 (section 3.1), because Typhoon T1807 was passing over the Sea of Japan north of the Chugoku region, no cold air flowed out to western Japan. Therefore, the horizontal gradient of potential temperature had not been strengthened in western Japan. After the passage of Typhoon T1807, a gradient zone of potential temperature was formed at around 34°N latitude by the outflow of cold air from the Okhotsk High. The southernmost isentropic surface, which was located at the tip of the gradient area of potential temperature and intersected the ground, was the 300 K isentropic surface. It is noteworthy that the isentropic surface of 300 K extended southward of western Japan before the arrival of the cold air from the Okhotsk High. The cold air outflow increased the vertical inclination of the 300 K surface.

3. Description of Fig. S3

Figure S3 illustrates LCL and LFC, when the air parcel at an altitude of 100 m was lifted above, averaged from 12 UTC on 5 to 00 UTC on 6 July in FLAT and NOEVAP_FLAT. The LCL of the warm air on the windward side of the frontal surface was about 400 m in FLAT and about 500 m in NOEVAP_FLAT, respectively. This is consistent with the bottom of the strong heating area extended vertically due to condensation (Figs. 13a, b). The LFC of the warm air on the windward side of the frontal surface was more than from 1000 m to 1500 m in both FLAT and NOEVAP_FLAT.

4. Description of Fig. S4

To show the shift of the ascending area corresponding to the northward shift of the inclined frontal surface, we conducted a forward trajectory analysis of the low-level warm moist air. In FLAT and NOEVAP_FLAT, trajectories were calculated for 12-h; 189 parcels were initially located at (x,y,z) (x represents one of 21 values from 130.5°E to 132.5°E with an interval of 0.1°E; y represents one of three values from 31.5°N to 32.5°N with an interval of 0.5°N; z represents one of three values from 0.1 km to 0.5 km with an interval of 0.2 km) at 12 UTC on 5 July. Data used in this calculation had a time interval of 3 min. We calculated the trajectories using Runge–Kutta fourth-order method with the integration time step of 1 min. Figure S4 presents three-dimensional forward trajectories and their projections to the surface for two experiments: FLAT and NOEVAP_FLAT. Air parcels were transferred northeastward at a low level, lifted up rapidly near the heavy precipitation area, and transferred east-northeastward in the middle troposphere. The active ascending area was located at higher latitudes in NOEVAP_FLAT than in FLAT. The two-dimensional surface projection illustrates clearly that the parcels reached higher latitudes in NOEVAP_FLAT than in FLAT.

5. Description of Fig. S5

Figure S5 portrays diabatic heating because of radiation processes and the difference between air temperature at 50 m and SST. From a comparison of Fig. S5a to Fig. 13a, one can confirm that a radiative cooling area exists near the top of the condensation heating paired with a cooling area over the Sea of Japan (38°

– 40°N). This radiative cooling is regarded as cooling by long-wave radiation from near the top of the lower cloud extending over the Sea of Japan. In addition, SST was about 1–2 K higher than the air temperature over the Sea of Japan (Fig. S5b). Therefore, the lower clouds are regarded as having been formed and maintained in the lower atmosphere destabilized by the radiative cooling near the top of the clouds and heating from the sea surface.

List of Figures

Fig. S1 Daily averages of contributions to the temporal change in cold airmass amounts below the 299 K surface due to the (a), (b) first and (c), (d) second terms in the right-hand side in Eq. (6) on 5 and 6 July 2018, respectively. The gray shaded area is the undefined area below ground level.

Fig. S2 Meridional vertical cross-sections of potential temperature averaged from 132° to 135°E every 12 h from 00UTC on 4 to 12UTC on 5 July 2018 in CNTL. The solid red line in each figure represents the 300 K isentropic line. The vertical range shown in this figure is from 1000 hPa to 850 hPa.

Fig. S3 Lifting condensation level (LCL, a: FLAT, b: NOEVAP_FLAT) and level of free convection (LFC, c: FLAT, d: NOEVAP_FLAT), when the air parcel at an altitude of 100 m was lifted above, averaged from 12 UTC on 5 to 00 UTC on 6 July. The white shaded area is the undefined area.

Fig. S4 Forward trajectories [(a) FLAT, (c) NOEVAP_FLAT] and its projection to the surface [(b) FLAT, (d) NOEVAP_FLAT] for 12 h from 12 UTC 5 to 00 UTC 6 July 2018. Note that figures (a) and (c) illustrate trajectories below an altitude of 2 km to focus on a flow at the lower layer.

Fig. S5 (a) Meridional vertical cross-section of diabatic heating (K day^{-1}, colored) because of radiation processes in FLAT, averaged for 132-135°E from 12 UTC on 5 to 00 UTC on 6 July. (b) Differences between air temperatures at 50 m altitude averaged from 12 UTC on 5 to 00 UTC on 6 July and sea surface temperature on 5 July.

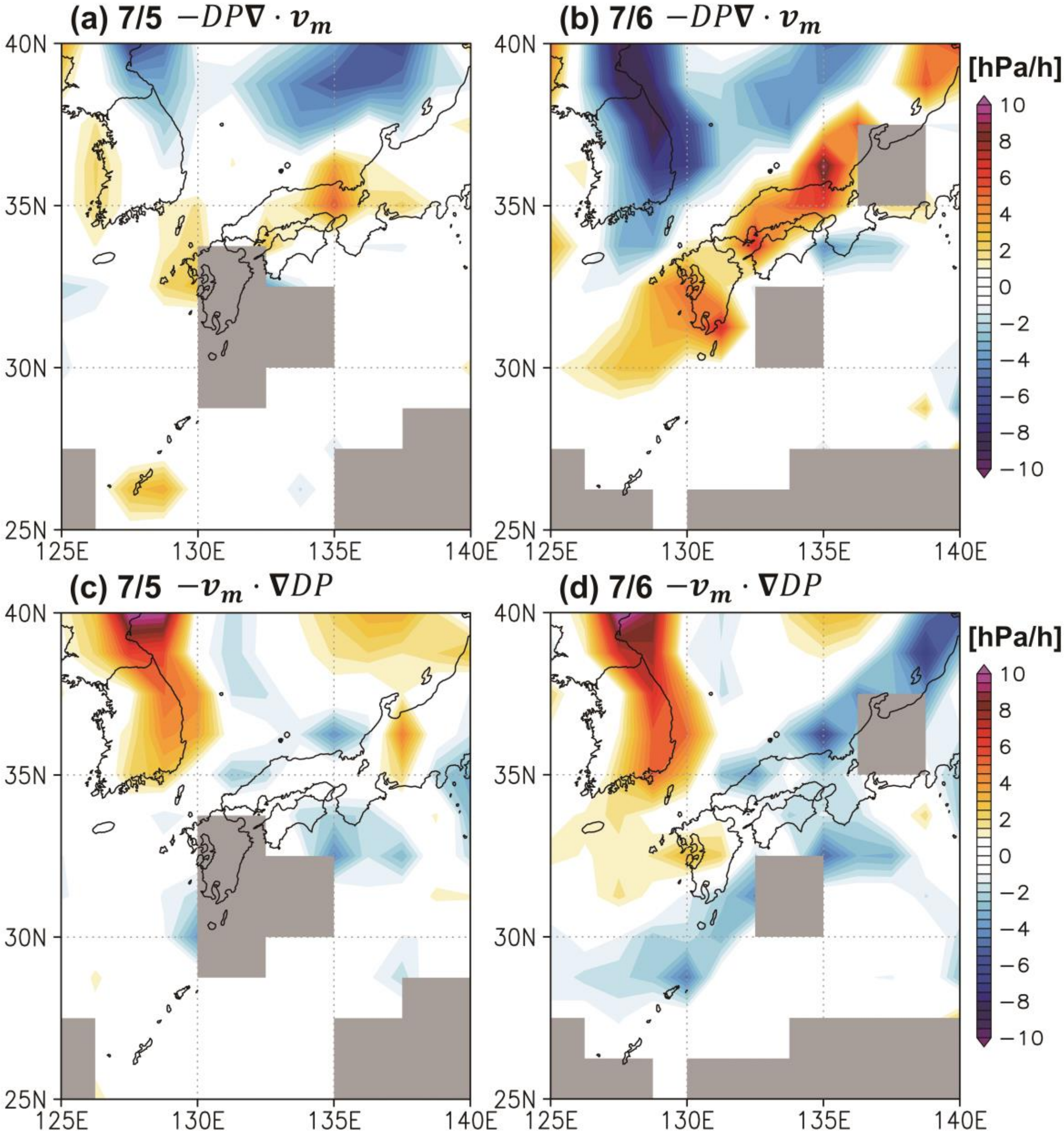

Fig. S1 Daily averages of contributions to the temporal change in cold airmass amounts below the 299 K surface due to the (a), (b) first and (c), (d) second terms in the right-hand side in Eq. (6) on 5 and 6 July 2018, respectively. The gray shaded area is the undefined area below ground level.

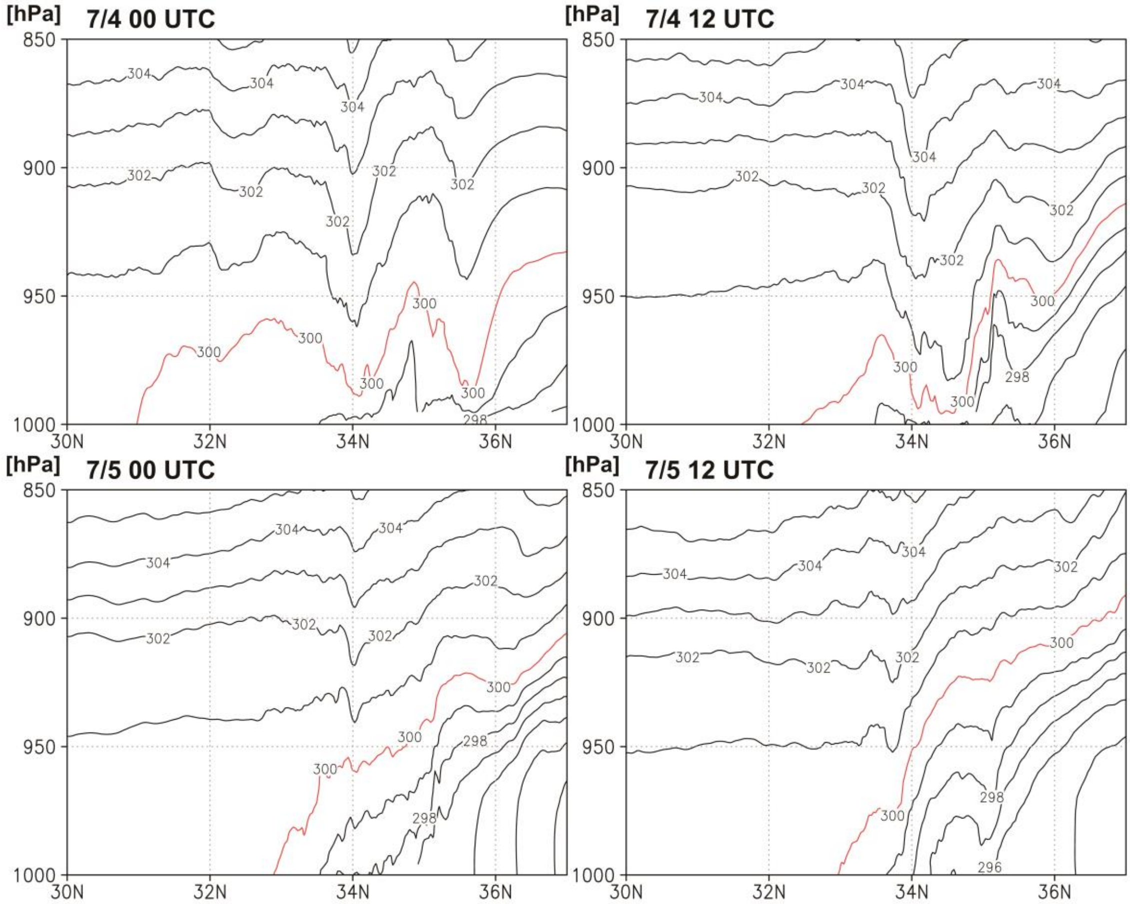

Fig. S2 Meridional vertical cross-sections of potential temperature averaged from 132° to 135°E every 12 h from 00UTC on 4 to 12UTC on 5 July 2018 in CNTL. The solid red line in each figure represents the 300 K isentropic line. The vertical range shown in this figure is from 1000 hPa to 850 hPa.

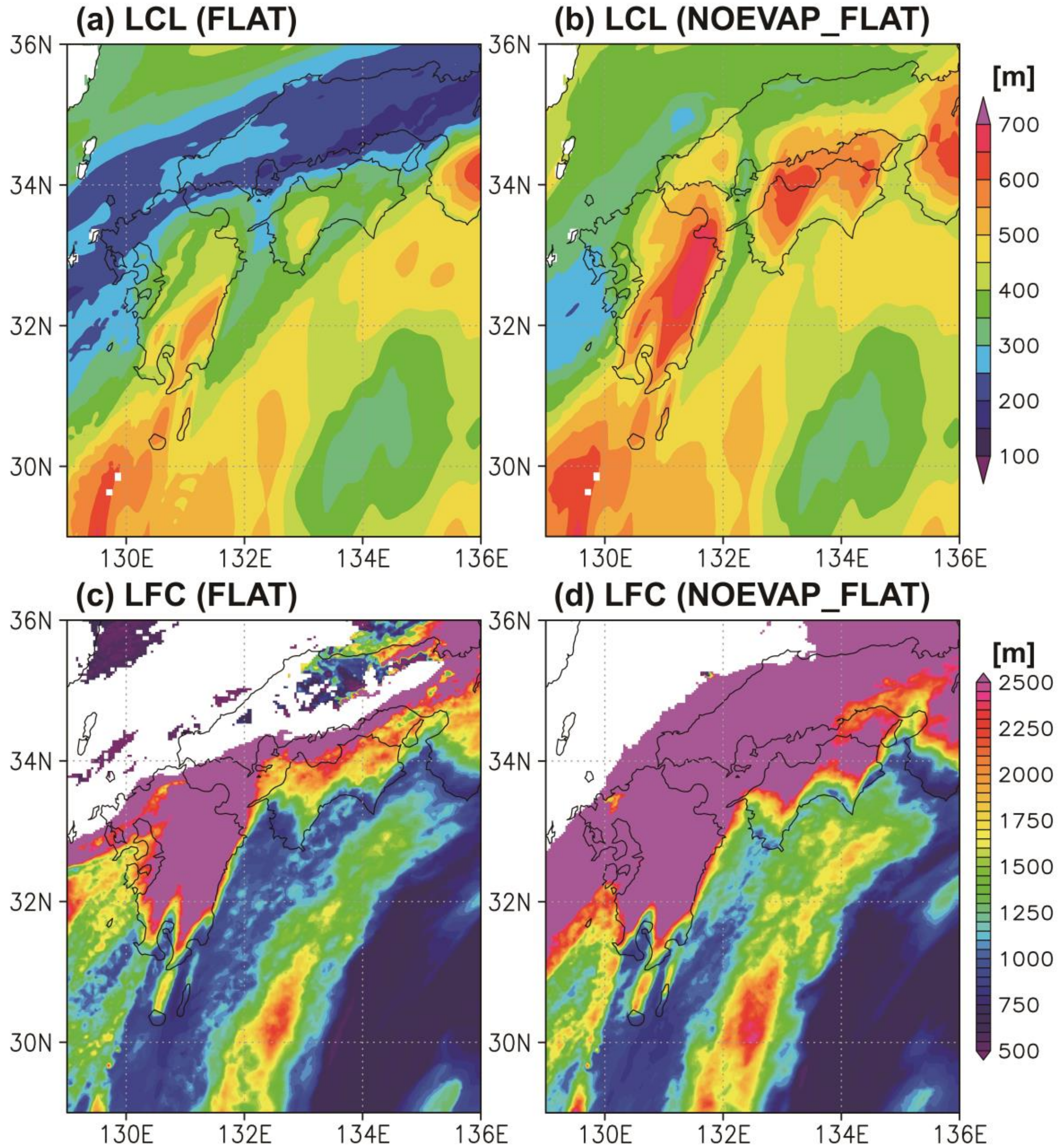

Fig. S3 Lifting condensation level (LCL, a: FLAT, b: NOEVAP_FLAT) and level of free convection (LFC, c: FLAT, d: NOEVAP_FLAT), when the air parcel at an altitude of 100 m was lifted above, averaged from 12 UTC on 5 to 00 UTC on 6 July. The white shaded area is the undefined area.

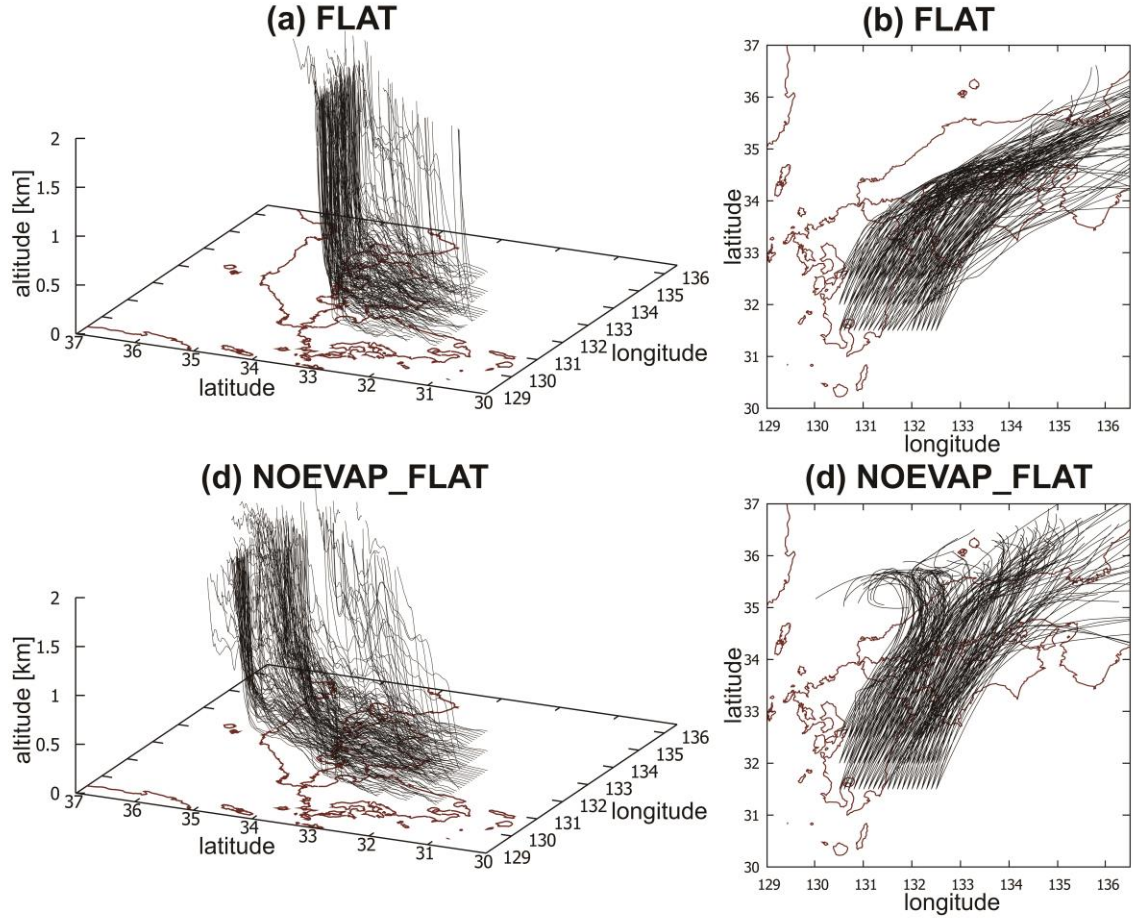

Fig. S4 Forward trajectories [(a) FLAT, (c) NOEVAP_FLAT] and its projection to the surface [(b) FLAT, (d) NOEVAP_FLAT] for 12 h from 12 UTC 5 to 00 UTC 6 July 2018. Note that figures (a) and (c) illustrate trajectories below an altitude of 2 km to focus on a flow at the lower layer.

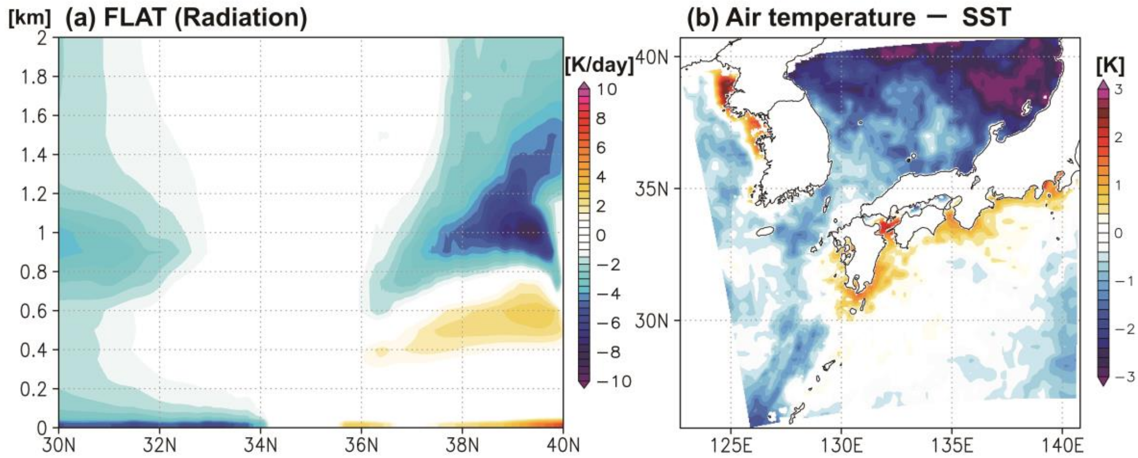

Fig. S5 (a) Meridional vertical cross-section of diabatic heating (K day^{-1}, colored) because of radiation processes in FLAT, averaged for 132-135°E from 12 UTC on 5 to 00 UTC on 6 July. (b) Differences between air temperatures at 50 m altitude averaged from 12 UTC on 5 to 00 UTC on 6 July and sea surface temperature on 5 July.